2606

UV generation in a pure silica holey fiber

J. H. V. PRICE[1], T. M. MONRO[1], K. FURUSAWA[1], W. BELARDI[1], J. C. BAGGETT[1], S. COYLE[2], C. NETTI[2], J. J. BAUMBERG[2], R. PASCHOTTA[3], D. J. RICHARDSON[1]

[1]*Optoelectronics Research Center, University of Southampton, SO17 1BJ, U.K.*

Fax: +44 23 8059 3142

Email: jhvp@orc.soton.ac.uk

[2]*Department of Physics and Astronomy, University of Southampton, SO17 1BJ, U.K.*

[3]*Ultrafast Laser Physics, Institute of Quantum Electronics,ETH Hönggerberg, Zurich, Switzerland*

Abstract: We report supercontinuum generation extending to 300 nm in the UV from a pure silica holey fiber. The broad spectrum was obtained by launching ultra-short pulses (~150fs, 10nJ at 820nm) from an amplified Ti:sapphire laser. The extension of holey fiber based supercontinuum generation into the UV should prove to be of immediate application in spectroscopy. By slightly detuning the launch conditions we excited a higher order spatial mode which produced a narrower supercontinuum, but with enhanced conversion efficiency at a series of blue/UV peaks around 360nm. We present numerical simulations, which suggest that differences in the dispersion profiles between the modes are an important factor in explaining this enhancement. In a related experiment, using the same laser source and fiber, we demonstrated visible supercontinuum from several subsidiary cores, with distinct colours in each core. The subsidiary cores were excited by appropriate input coupling. Fabrication of a fiber with a range of core sizes (dispersion profiles) for tailored supercontinuum generation can therefore be envisaged for practical applications.

PACS: 42.72.Bj, 42.79.Nv, 42.81.Dp

Keywords: *Holey fiber, Microstructured fiber, UV, supercontinuum*

1. Introduction

Microstructured "holey" fibers have a unique range of optical properties [1,2] and have enabled new applications in spectroscopy [3], metrology [4] and

communications [5,6]. Although the field of supercontinuum research using conventional fibers has been active for many years at wavelengths near 1.5 μm for telecommunications applications [7], the unique properties of holey fibers have enabled the demonstration of visible supercontinuum in holey fiber pumped directly with a Ti:sapphire oscillators [8]. This demonstration encouraged tremendous new research interest to both explain the origin of this remarkable spectral broadening [9,10] and to develop further applications [11]. Visible supercontinuum spectra have previously been reported spanning 390-1600 nm using microstructured holey fiber [8,9], and 375-1500 nm [12] using tapered standard fiber. However there is strong interest in extending the achievable bandwidths still further, particularly towards the ultraviolet (UV) regions of the spectrum [13,14] for use in spectroscopy.

In this paper, we report what we believe is the first detailed investigation of holey fiber based UV generation via supercontinuum spectral broadening at wavelengths below 350 nm pumped from a mode-locked Ti:sapphire source. We report UV generation at wavelengths at least as short as 300 nm. We demonstrate that coupling into a higher order spatial mode produces enhanced UV intensity in a series of peaks near 360 nm. We believe this is the first demonstration of multiple spectra using different core modes of a single fiber from a single pump source.

The dispersion profile of a holey fiber has been shown [10] to strongly influence the spectral shape of the supercontinuum produced. We present, for the first time to our knowledge, full vector calculations based on the scanning electron-micrograph (SEM) of an actual fiber structure, of the dispersion characteristics of the higher order spatial modes that were observed to produce enhanced UV generation. Our calculations show that the zero dispersion wavelength (λ_0) is close to the pump wavelength for the fundamental mode for our fiber, but at significantly shorter wavelengths for the higher order modes. We have used these dispersion profiles to perform numerical simulations of the continuum spectra in the fundamental and higher order modes, and which

are in reasonable agreement with the measured spectra. Our observation that pumping close to λ_0 creates a broad flat spectrum, whereas pumping above λ_0 creates both red-shifted and blue-shifted spectral bands, is consistent with the investigations of other authors [10] into the continuum spectra from the fundamental spatial mode made using fibers with different core sizes, and hence dispersion profiles.

Finally, using the same fiber and laser source, we demonstrated that by varying the input coupling appropriately, visible supercontinuum from several subsidiary cores could be produced. The colours of the supercontinuum spectra differed for each subsidiary core, which we consider was due to differences between the dispersion profiles of each core and also to differences between the input coupling efficiencies. This initial demonstration of supercontinuum generation in a multi-core fiber shows the potential for designing a fiber with an array of cores with different dimensions (dispersion profiles) and that could be selectively excited for tailored spectral generation from a single fiber structure.

The choice of fiber material is important for efficient UV generation in order to avoid unacceptable absorption (attenuation). High UV transmission losses affect standard silica based fibers, which are used to fabricate tapers for supercontinuum generation, because the ions typically incorporated in the fiber core in order to obtain the required transverse refractive index profile result in strong absorption in the UV (e.g. germanium doped silica has ~10,000 dB/km stronger absorption [15] at 250 nm compared to pure (undoped) silica). We expect that the comparatively low material loss of the single material pure silica holey fiber as used in the experiments presented here should make such fibers strong candidates for efficient fiber-based UV supercontinuum sources.

This paper is structured as follows. In Section 2 we describe the details of the experiment, and the properties of the holey fiber. In Section 3, we describe our numerical simulations and compare the results to our experimentally

measured spectra. In Section 4 we report our observations of supercontinuum generation in several subsidiary cores of the fiber, and in Section 5 we draw our conclusions.

2. Experimental observation of UV supercontinuum

Supercontinuum generation was produced by coupling high energy ultrashort pulses into a short length of holey fiber. A schematic of our experimental setup is shown in Fig. 1. The supercontinuum generation at visible and near infrared wavelengths was recorded using a fiber-coupled optical spectrum analyzer, whereas a UV-optimised spectrometer and cooled CCD were used for wavelengths extending to below 300nm. The spectral data presented in this paper were produced using a pump wavelength λ_{pump}=820nm. Coupling into the fundamental mode, which has a zero-dispersion wavelength (λ_0) close to λ_{pump}, produced a yellow coloured supercontinuum, but by coupling into a higher order mode, we produced a dramatic change in the colour of the supercontinuum to bright blue-white, and we recorded UV spectra for the two-lobed mode showing power transferred to a series of peaks around 360 nm. By pumping at a shorter wavelength, we produced a wider variety of colours in higher order modes, as shown in Fig. 4.

Figure 1

This section is structured as follows: Section 2.1 describes the characteristics of the holey fiber. Section 2.2 presents the results showing UV generation to wavelengths as short as 300 nm in the UV. Section 2.3 shows the results obtained by coupling into higher order spatial modes (enhanced conversion efficiency into UV peaks). Section 2.4 is a brief report of our observations of laser induced damage to the fiber input facet.

2.1 Properties of the holey fiber

A SEM image of our robust, jacketed, polarization-maintaining holey fiber is shown inset to Fig.1. Holey fibers with a small core and large air fraction cladding have a greatly reduced mode area (typically ~30-50 times smaller compared to Corning SMF28 fiber), which increases the effective nonlinearity and drastically reduces the zero dispersion wavelength down to visible wavelengths [2] (compared to the minimum of 1.3 μm obtainable from standard single-mode fiber [16]). The fiber has a ~1.6 μm diameter core, and a large air fill fraction in the cladding and this combination results in a highly confined mode with $A_{eff} \sim 2.5\ \mu m^2$. The fiber is rigorously single mode at wavelengths above 1μm, but supports higher order modes at shorter wavelengths.

As mentioned in the introduction, we observed supercontinuum generation in higher order spatial modes, which was accompanied by enhanced spectral conversion in strong UV peaks. To further understand this process, we have calculated the mode area and dispersion properties of the fundamental and next lowest order fiber modes as shown in Fig. 2. The calculated dispersion profiles (Fig. 2(b)) show that the two polarisation modes (quasi-linearly polarized) associated with each transverse mode are not degenerate because the asymmetry of the fiber profile leads to mode splitting. (By comparison, these pairs of quasi-linearly polarized modes would remain degenerate for a fiber with an idealized hexagonal hole configuration [17].) It is therefore crucial to use a full vectorial method to calculate the properties of this small-core fiber, and we used a full vectorial implementation of the orthogonal function method [1,18] incorporating both odd and even functions to describe the modal fields and holey fiber profile. The material dispersion of silica is incorporated in the calculations directly via use of the Sellmeier equation. The numerically predicted intensity profiles of the two-lobed spatial modes, and near field photographs of continuum generation in each mode are shown

in Fig. 2(a),(d). (A 100x microscope objective was used to image the fiber output onto a screen.) The predicted intensity profiles match the observed mode-shapes well, including details of the asymmetries in each direction. The dispersion predictions for the two-lobed modes and for the fundamental mode are presented in Fig. 2(b). The three pairs of different dispersion profiles (hence different λ_0) create distinctive supercontinuum spectral shaping. The zero dispersion wavelengths are: λ_0 = 795 nm, 838 nm (polarisation dependent) for the fundamental mode; λ_0 = 611 nm, 629 nm (polarisation dependent) for the mode of Fig. 2(a); and λ_0 = 671 nm, 694 nm (polarisation dependent) for the mode of Fig. 2(d). The injection wavelength used in our experiments (λ_{pump}= 820 nm) is shown in Fig. 2(b). The calculated effective mode area (A_{eff}) of the fundamental mode is shown in Fig. 2(c). We also calculated A_{eff} of all six modes to be: 2.32 μm^2, 2.43 μm^2 for the two principal polarisation axes of the fundamental mode; 2.01 μm^2, 2.05 μm^2 for the mode of Fig. 2(a); and 2.34 μm^2, 2.38 μm^2 for the mode of Fig. 2(d) (all calculated at a wavelength of 675 nm, which is close to the centre of the observed supercontinuum spectra).

Figure 2

The measured loss of the fiber (fundamental mode) is ~40dB/km at a wavelength of 1.55μm [5]. However single material holey fibers with losses as low as 0.58dB/km at λ= 1.55 μm have been fabricated [19], and therefore excess loss should not be a constraint on the performance of future practical devices based on this technology. Calculations based on the multipole method [20] indicate that confinement loss provides a significant contribution toward the total measured loss in this fiber, but that it should be possible to reduce the confinement loss for this fiber to well below 0.1dB/km simply by adding more rings of air holes. In any fiber, higher order modes extend further into the

cladding, and therefore have a higher associated confinement loss. Although detailed measurements and predictions have not been made for the higher order modes of the fiber used here, it is anticipated that these modes would experience very large confinement loss, and so would not be observable in long fiber lengths. This effect was observed experimentally because for the mode of Fig. 2(a), which has λ_0 and A_{eff} furthest from those of the fundamental mode, we could much more easily observe transmitted power through a 15cm fiber length compared to a 25 cm fiber length, whereas we observed the mode of Fig. 2(d) through a longer length of fiber without difficulty.

2.2 Broadband supercontinuum generation extending into the UV

In this section we describe our experimental setup and the special precautions used to make measurements in the UV. The experimental arrangement is shown in Fig. 1. High energy, ultrashort (~150fs FWHM) pulses at a wavelength of 820nm from a mode-locked Ti:sapphire laser system (TEM_{00} mode, average power~ 10 mW, repetition rate = 250 kHz) were launched into a ~25cm length of holey fiber using a 40x microscope objective. By maximising the coupling efficiency, we launched ~25% of the incident power (launched energy ~10 nJ, peak power ~50 kW). The supercontinuum at the fiber output was recorded at visible and near infrared wavelengths using a fiber-coupled optical spectrum analyzer (ANDO AQ6315B), and using a UV optimised spectrometer (appropriately blazed diffraction grating; UV enhanced CCD detector) for wavelengths at least as short as 300 nm. We used UV fused silica (UVFS) lenses to couple light into the spectrometer in order to avoid the poor transmission of standard BK7 glass lenses at short wavelengths.

Fig. 3.(a) shows the observed supercontinuum extending from <300 nm to >1600 nm and combines the data from the optical spectrum analyzer and

spectrometer. We have considered the wavelength variation of the spectrometer efficiency, calculated from the efficiency curves of each spectrometer element shown in Fig. 3(b). The overall spectrometer efficiency was found to be approximately uniform from ~250 nm to 800 nm, so we have not adjusted the UV spectra of Fig. 3(a),(d) for instrument variation. The spectrometer slit width was held constant to minimise variations in spatial mode filtering. Scatter from higher order diffraction of the pump (820nm) and longer wavelengths was removed using a UG1 coloured filter from Schott Glass, which blocks most wavelengths >600 nm. Fig. 3 (c) shows the overall efficiency of the spectrometer with and without the filter. The differences between the filtered and unfiltered spectra should comprise: (i) weak attenuation at the measured UV wavelength, and (ii) strong attenuation of longer wavelengths, which removes potential false counts caused by 2nd order diffraction. Fig. 3(d) shows the UV spectra with and without the coloured filters. The differences between the filtered and unfiltered spectra match the absorption of the coloured filter at the UV wavelength, so we concluded that scatter from higher order diffraction of long wavelengths was not distorting the unfiltered spectrum. The measurements therefore confirm that the supercontinuum spectrum extends down to at least 300 nm in the UV.

For the supercontinuum produced in the fundamental mode of our fiber (λ_0 close to λ_{pump}), we interpret our observation of UV generation to 300 nm, which represents a more extreme broadening towards the UV than typically reported [8,10], to result from differences between the precise form of the dispersion profile of our fiber compared to the fibers studied by other authors, and perhaps also from our detailed observations using a spectrometer with enhanced sensitivity in the UV.

Figure 3

2.3 Enhanced UV generation in higher order spatial mode

Despite the wide interest in supercontinuum research, there have been few previous reports of supercontinuum in higher order spatial modes [13,21,22]. Due to the large index difference between core and cladding modes of small core, high air fill fraction holey fibers, the effective index of the fundamental mode, which is mostly confined within the core, is substantially greater than for higher order modes, which extend into the holey cladding. It is therefore comparatively difficult to couple to higher order modes of these holey fibers, and the perturbations which couple modes in standard fibers (small variations of core diameter resulting from fabrication, and bending of the fiber) are comparatively less effective at mode-mixing. However, Fig. 4 illustrates that by slightly detuning the pump launch from that for optimal launch efficiency, we obtained strong coupling into higher order spatial modes accompanied by a visually stunning change in the color of the fiber output from pale yellow (Fig. 4(b)(ii)) to bright white(Fig. 4(b)(iii)), which led us to investigate the supercontinuum spectrum into the UV.

Using a pump wavelength of ~820 nm produced only the fundamental mode of Fig. 4(b)(ii), or the two-lobed mode oriented as shown in Fig. 4(b)(i),(iii). We observed that the mode-colour of Fig. 4(b)(iii) was associated with the strongest UV generation. Using an OPA system to provide a pump wavelength of ~675 nm (similar pulse energy and duration compared to 820 nm pulses), we observed a wider range of colours produced in higher-order modes and with lobes in either orthogonal orientation as shown in Fig. 4(b) (iv)-(vi) . The relative ease of generating supercontinuum in higher order modes when $\lambda_{pump} = 675$ nm (compared to $\lambda_{pump} = 820$ nm) could be because the pump wavelength is then closer to λ_0 of the higher order modes, although we have not identified the exact mechanism.

The average power transmitted in the higher order modes was typically ~1mW, compared to ~2mW in the fundamental mode. The reduction in transmitted power is due to lower launch efficiency (off-axis launch) and to somewhat higher transmission losses in this higher order-mode, but high energy pulses (up to 5nJ) could still be launched into this higher order mode. The orientation of the two-lobed mode was predominantly that shown in Fig. 4(b)(iii), which corresponds to the mode of Fig. 2(d).

Figure 4

Coupling into the two-lobed mode of Fig. 4.(b)(iii) resulted in an enhancement of the power at wavelengths close to 360nm, and a narrowing of the supercontinuum. Fig. 5. (top) shows the results from coupling into the two lobed spatial mode (shown inset). Fig. 5. (lower) shows the results from coupling into the fundamental mode (shown inset). The spectrum from the two lobed mode (Fig. 5(a)(top)), , was narrower when compared to the spectrum from the fundamental mode (Fig. 5(a)(lower)), but retained strong spectral conversion to <450 nm wavelengths. Enhanced UV generation at a series of peaks near ~360 nm is demonstrated in Fig. 5(b) from the two-lobed mode (top plot), but the peaks are not present in the fundamental mode spectrum (lower plot). A set of neutral density filters was used to vary the input power, and which resulted in the increasing intensity levels shown in Fig. 5(b). As described in Section 2.2, we used coloured filters to block unwanted scatter from the longer wavelengths and that could otherwise distort the UV measurements.

Figure 5

2.4 Observation of laser-induced damage to the fiber tip

We observed that perturbations to the input launch conditions (e.g. caused by knocking gently on the optical table near the lens mount), could somehow change the fiber so that it was no longer possible to couple into the fundamental mode, but only into the two-lobed mode (which was associated with enhanced UV generation, as our previous measurements demonstrated). By re-cleaving the fiber tip to reveal a new facet we could again excite the fundamental mode. We suggest that our observations are due to optically induced damage to the fiber facet, which would cause the pump light to couple into the higher order mode for all launch configurations (although we have not identified the precise damage mechanism). This explanation would be consistent with reports from other groups [13] that significant UV generation was only obtained following melting of the fiber facet (as observed from SEM images) when using 1W incident average power from a high repetition rate source, but with pulse characteristics (FWHM~200 fs, energy ~ 14 nJ) similar to those used in our experiments.

3. Comparison of experimental results with numerical simulations

In this section, we compare the results of our numerical modeling to the experimentally measured spectra. We performed the modeling to provide insight into the mechanisms giving rise to the enhanced UV generation in the higher order spatial mode. When considering which parameters to include in the model, we first noted that in order to excite the higher order mode it was necessary to detune the launch with respect to that used for optimum coupling into the fundamental mode. In addition, the fibers used in our experiments were quite short (25 cm), so strong coupling between modes subsequent to launch would be unlikely. We therefore considered that coupling into the two-lobed mode occurred solely at launch, and not by mode-mixing from the

fundamental mode after launch. This suggested that the properties (nonlinearity, dispersion) of the two-lobed mode alone could be responsible for the spectral shaping, rather than a more complex inter-modal process. As described in Section 2.1, the effective mode areas of the fundamental and two-lobed mode are very similar, implying similar effective nonlinearities for these modes. However, the dispersion properties are dramatically different; in particular, the two-lobed mode has λ_0~690 nm compared to λ_0~810 nm for the fundamental mode. The shorter λ_0 of the higher order mode would cause phase-matching to transfer energy further towards the UV, and would explain the general observation of enhanced UV generation.

To support our suggestion that the difference between the supercontinuum produced in different spatial modes is principally due to differences between the dispersion profiles of those modes, we performed numerical simulations based on the dispersion profiles for those modes. Our numerical model (ignoring fiber losses) uses a generalized scalar propagation equation suitable for use in studying broadband pulse evolution, and used by other authors in the field [23,24],

$$\frac{\partial A}{\partial z} - i\sum_{k\geq 2}\frac{i^k \beta_k}{k!}\frac{\partial^k A}{\partial t^k} = i\gamma\left(1+\frac{i}{\omega_0}\frac{\partial}{\partial t}\right)\otimes\left[A(z,t)\int_{-\infty}^{t} R(t')\left|A(z,t-t')\right|^2 dt'\right]$$

where $A = A(z,t)$ is the electric field envelope, β_k are the dispersion coefficients at the center frequency ω_0, $\gamma = n_2\omega_0/(cA_{eff})$ is the nonlinear refractive index, and A_{eff} is the effective area of the fiber. The right-hand side of the propagation equation models the effects of the nonlinear propagation, including self-phase modulation, self-steepening, optical shock formation, and intra-pulse Raman scattering. The response function $R(t) = (1-f_R)\delta(t) + f_R h_R(t)$ includes both instantaneous and delayed nonlinear response of the fiber, where $f_R = 0.18$ is the fractional contribution of the Raman delayed response. For h_R, we used the experimentally

determined Raman response of silica. To solve the propagation equation, we used a standard split-step Fourier algorithm treating dispersion in the frequency domain and the nonlinearity in the time domain, apart from the temporal derivative for the self-steepening effect, which is evaluated using Fourier transforms.

We used the dispersion and A_{eff} data from Section 2.1, and chose parameters for our launched pulses that would correspond to the experimentally observed average transmitted power from the fiber (E ~10 nJ, in the fundamental mode, E ~ 5nJ, in the two-lobed mode; λ_{pump} = 820 nm, FWHM ~150 fs for both modes). We also performed simulations for pulses with half of these energies and the results were qualitatively similar, with only slight variations in the bandwidth. Our simulation results show the expected [24] spectral fine structuring and we have applied a rolling average to smooth the data, which is then approximately comparable to the time averaged experimental measurements. We present simulation results for one of the principal polarisation axes, but the results were qualitatively similar for the other axis. We note that there are further refinements that can be made to the above NLSE to include effects such as loss along the fiber length, ultraviolet and infrared absorption bands, polarisation coupling, and the wavelength dependence of the effective mode area. However, the simulations show reasonable qualitative agreement with the experimental spectra.

The results of our simulations (red) and the experimental data (black) are shown in Fig. 6 for both the fundamental and the two-lobed modes. The simulation and experimental spectra show reasonable qualitative agreement: the simulation results for the fundamental mode show a broad, flat spectrum with approximate agreement to the experimentally observed bandwidth; and the simulation results for the higher order mode show a narrower spectrum, but with significant power at blue wavelengths. Given the complexity of the phenomenon of supercontinuum in higher order modes, and the approximations made in our simulations, exact agreement between simulations

and experimental observations could not be expected. However, the main features observed in our simulation results are consistent with our experimental spectra. Our simulation results are also consistent with both experimental and theoretical results from other groups [10] that have used fibers with different λ_0 in relation to the pump wavelength, but always in the fundamental spatial mode: i.e. pumping near λ_0 produced a broad, flat spectrum, and pumping on the anomalous dispersion side of λ_0 produced discrete red-shifted and blue-shifted bands.

Figure 6

Fig. 6 (b) shows that the principal difference between the simulation and experimental spectrum for the higher order mode is that the simulation shows a lower intensity near λ_0 (690nm). We suspect that the higher intensity observed experimentally is likely to arise due to a non-ideal launch into the higher order mode resulting in residual excitation of the fundamental mode, as shown by the photographs of Fig. 4 and Fig. 5. Similarly, for the spectrum of the fundamental mode shown in Fig. 6 (a), a small fraction of the launch power coupled into the higher order mode could be responsible for the shoulder in the experimentally observed spectrum at ~450nm that is not present in the simulation result (the simulations predict a peak in the higher order mode spectrum at approximately that wavelength). The simulations predict strong pump depletion such that there is no peak remaining at the pump wavelength. This is consistent with the simulations of other authors [9,21], and we suspect that the experimentally observed peak at the pump wavelength is due to a small fraction of the incident power guided by lossy cladding modes and observed because the fiber length is short. Overall, we believe that the simulation results provide support for our suggestion that the difference in general form of the supercontinuum spectra is principally due to

the differences between dispersion profiles of the fundamental and two-lobed modes.

4. Supercontinuum generation in subsidiary cores

In this section we describe our observations from a related experiment that produced supercontinuum in several subsidiary cores of the fiber. Examples of multiple core holey fibers that have previously been reported include a dual core holey fiber [25], and a holey fiber containing several cores of different dimensions [26]. However, this is the first time, to our knowledge, that supercontinuum generation in secondary cores of a holey fiber has been demonstrated. In the fiber used here, the "subsidiary" cores arise where imperfections in the structure have created relatively thicker regions of silica. In the future, it would be straightforward to envisage the systematic fabrication of multiple cores using additional solid cores in the capillary stacking process. The experimental arrangement was similar to that used for continuum generation in the higher order modes of the principal core (Fig. 5(a).), using the same pump pulses and holey fiber, but with more extreme detuning of the launch.

Fig. 7(a) shows a typical far-field mode shape produced by continuum in a subsidiary core, observed as scattered light from a white card a few centimeters from the fiber end; the six-fold symmetric pattern in a uniform colour is surprising because the fiber does not have a perfectly regular hexagonal structure, and it is substantially different from the far field images of higher order modes in the principal core (Fig. 4). However, the observed geometric nature of the far field modes was characteristic of our observations of continuum generation in subsidiary cores.

Fig. 7(b)-(d) shows near-field pictures of supercontinuum in subsidiary cores that were recorded using a 100x microscope objective to focus the fiber output

onto a screen. Using a camera on a tripod, we recorded all the near-field images from the same relative position, and we then matched the images to the subsidiary cores by overlaying those images onto the SEM of the fiber. In contrast to the far-field image, the near-field images show that the mode shapes clearly follow the fiber structure; the modes in Fig. 7(c),(d) spread into neighboring subsidiary-cores where the struts are broad, and thus the subsidiary core modes are poorly confined.

Figure 7

Fig. 7(b)-(d) demonstrates that characteristic colours were produced by each core. The colours in any core changed when a half-wave plate was used to rotate the plane of polarisation of the input pulses. The dispersion of a holey fiber has been shown [10,27] to be a controlling factor for supercontinuum spectral broadening, and we interpret the distinctive colours associated with each subsidiary core to be an indication of the different dispersions of these cores. The size of all the subsidiary cores (~1 μm) was of the same scale as the guided wavelengths, so we would expect the waveguide dispersion to be a sensitive function of the precise core dimensions. The strong asymmetry of the subsidiary cores also leads to substantially different dispersion properties for the orthogonal polarisation axes, which would cause the continuum colour to change with variations of the input polarisation.

We also considered the increased losses of these subsidiary cores. In an idealized holey fiber, the average refractive index of the periodically arranged cladding, is lower than the refractive index of the solid core region, and so light is guided by this effective refractive index difference (Δn). As explained [20] in Section 2, reducing the confinement losses for small core holey fibers (to the few dB/km) requires a sufficient diameter of holey (microstructured) cladding around each core (number of rings of holes). It has previously been empirically determined [26] that in order to confine light of wavelength λ, all fine silica struts surrounding a subsidiary core must be longer than ~2λ, and

narrower than ~1.2λ. The supporting struts in our fiber were short and wide compared to the wavelength of the guided light, and the confinement losses of the subsidiary cores were therefore high. The confinement losses were evident experimentally because the fiber glowed much more brightly (unguided light) when continuum was produced in subsidiary cores compared to when continuum was produced in the main core. Furthermore, we only observed the supercontinuum in subsidiary cores using a short fiber length (15 cm as opposed to a 25 cm length for our other measurements). The average power transmitted through the fiber in subsidiary cores was ~0.5 mW compared to ~2.5 mW in the central core, due to a combination of the increased confinement losses and the reduced launch efficiency. However, we suggest that it should be possible to dramatically reduce excess losses by choosing an appropriately designed fiber structure.

Overall, we believe that this initial observation if supercontinuum generation in several subsidiary cores of a holey fiber demonstrates the potential for fabrication of a fiber with several cores of different dimensions for tailored continuum generation from a single fiber.

5. Conclusion

In conclusion, we have demonstrated supercontinuum generation from 300 nm in the UV to above 1600 nm in the IR from a pure-silica holey fiber. Care was taken to consider the efficiency of our UV enhanced spectrometer across the blue/UV spectral range, and we used coloured glass filters to block unwanted scatter from longer wavelengths. By coupling into a two-lobed spatial mode, we measured substantially enhanced UV generation in a series of blue/UV peaks at wavelengths near 360nm. Since the fiber lengths used in our experiment were quite short (~15cm), and because it was necessary to detune the launch in order to couple into the two-lobed mode, we believe that the enhanced UV results from differences in the dispersion profiles of the fundamental and higher order two-lobed modes. To enhance our

understanding of this process, we used a full vector model based on the SEM of the fiber structure to calculate the dispersion profiles for the fundamental mode, and for the two orthogonally oriented two-lobed modes, and we performed numerical simulations of supercontinuum spectra produced by these dispersion profiles. The simulation and experimental results are in reasonable qualitative agreement, which provides support for our suggestion that the enhanced UV generation is due in large part to the differences in the dispersion profiles of the distinct spatial modes.

We have also demonstrated visible supercontinuum with distinct colours produced in several subsidiary cores of our multi-core fiber. We interpret the different colours produced by each subsidiary core to result from variations in the dispersion profiles of the cores (and from the reduced launch efficiency). We believe that the extension of holey fiber based supercontinuum generation into the UV will prove to be of immediate practical application in spectroscopy. Following the results presented here, we could envisage the design of a fiber with optimised dispersion characteristics for enhanced UV generation. Power scaling to generate substantial UV intensity should be possible by using a higher repetition rate system compared to the 250 kHz source used in these experiments; and any such work would ideally consider new pump wavelengths in order to exploit more practical sources for supercontinuum generation based on diode-pumped ytterbium-doped fiber amplifiers [28]. Following our demonstration of supercontinuum in several subsidiary cores, it is now possible to consider the fabrication a fiber specifically designed with a selection of multiple cores with different dimensions to enable several tailored supercontinuum spectra to be generated from a single holey fiber.

Acknowledgments:

It is a pleasure to thank Neil Broderick and Vittoria Finazzi for illuminating discussions. J. Price and J. C. Baggett acknowledge the support provided by the Engineering and Physical Sciences Research Council, UK, (EPSRC)

during the course of this research. T. M. Monro is supported by the Royal Society through the University Research Fellowship Scheme. This research was supported by the EPSRC, research grant number GR/N37261 and HEFCE grant number JR9850BA.

References

1. T. M. Monro, D. J. Richardson, N. G. R. Broderick, P. J. Bennett: J. Lightwave Technol. **17,** 1093 (1999)
2. J. C. Knight, J. Arriaga, T. A. Birks, A. Ortigosa-Blanch, W. J. Wadsworth, P. St.J.Russell: IEEE Photonics Technol. Lett. **12,** 807 (2000)
3. R. Holzwarth, T. Udem, T. W. Hansch, J. C. Knight, W. J. Wadsworth, P. St.J.Russell: Phys. Rev. Lett. **85,** 2264 (2000)
4. D. J. Jones, S. A. Diddams, J. K. Ranka, A. Stentz, R. S. Windeler, J. L. Hall, S. T. Cundiff: Science **288,** 635 (2000)
5. J. H. Lee, Z. Yusoff, W. Belardi, M. Ibsen, T. M. Monro, D. J. Richardson: Opt. Lett. **27,** 927 (2002)
6. Z. Yusoff, J. H. Lee, W. Belardi, T. M. Monro, P. C. Teh, D. J. Richardson: Opt. Lett. **27,** 424 (2002)
7. H. Takara, T. Ohara, K. Mori, K. Sato, E. Yamada, Y. Inoue, T. Shibata, M. Abe, T. Morioka, K. I. Sato: Electron. Lett. **36,** 2089 (2000)
8. J. K. Ranka, R. S. Windeler, A. J. Stentz: Opt. Lett. **25,** 25 (2000)
9. A. V. Husakou, J. Herrmann: Phys. Rev. Lett. **8720,** 3901 (2001)
10. J. Herrmann, U. Griebner, N. Zhavoronkov, A. Husakou, D. Nickel, J. C. Knight, W. J. Wadsworth, P. St.J.Russell, G. Korn: Phys. Rev. Lett. **88** (2002)
11. P. Petropoulos, T. M. Monro, W. Belardi, K. Furusawa, J. H. Lee, D. J. Richardson: Opt. Lett. **26,** 1233 (2001)
12. T. A. Birks, W. J. Wadsworth, P. St.J.Russell: Opt. Lett. **25,** 1415 (2000)
13. A. Efimov, F. G. Omenetto, A. J. Taylor, J. C. Knight, W. J. Wadsworth, P. St.J.Russell: Conference on Lasers and Electro Optics (2002) Longbeach, California, May 19-24, 2002, paper CThL5
14. J. H. Price, K. Furusawa, T. M. Monro, C. Netti, A. Malinowski, J. J. Baumberg, D. J. Richardson: Conference on Lasers and Electro Optics (CLEO), Vol. 73 of OSA Trends in Optics and Photonics Series (Optical Society of America, Washington, D.C., 2002) paper CTuB5 (2002)
15. *Infrared Fiber Optics*, ed. by J. S. Sanghera, I. D. Aggarwal: (CRC Press, 1998)
16. G. P. Agrawal: *Nonlinear Fiber Optics*, 2nd ed. (Academic Press, San Diego, 1995)
17. M. J. Steel, T. P. White, C. M. de Sterke, R. C. McPhedran, L. C. Botten: Opt. Lett. **26,** 488 (2001)
18. T. M. Monro, N. G. Broderick, D. J. Richardson: Nanoscale Linear and Nonlinear Optics: International School on Quantum Electronics, Erice, Sicily, July 2000, ed. by M. Bertolotti, C. M. Bowden,C. Silbilia, (AIP, Melville, NY, 2000)
19. L. Farr, J. C. Knight, B. J. Mangen, P. J. Roberts: European Conference on Optical Communications (2002) Copenhagen, Denmark, September 8-12, 2002, Post-deadline paper PD1.3
20. V. Finazzi, T. M. Monro, D. J. Richardson: Optical Fiber Communications Conference (2002) Anaheim, California, March 17-22, 2002, paper ThS4
21. J. M. Dudley, L. Provino, N. Grossard, H. Maillotte, R. S. Windeler, B. J. Eggleton, S. Coen: J. Opt. Soc. Am. B-Opt. Phys. **19,** 765 (2002)
22. F. G. Omenetto, A. J. Taylor, M. D. Moores, J. Arriaga, J. C. Knight, W. J. Wadsworth, P. St.J.Russell: Opt. Lett. **26,** 1158 (2001)
23. G. Genty, M. Lehtonen, H. Ludvigsen, J. Broeng, M. Kaivola: Opt. Express **10,** 1083 (2002)
24. J. M. Dudley, S. Coen: Opt. Lett. **27,** 1180 (2002)
25. B. J. Mangan, J. C. Knight, T. A. Birks, P. St.J.Russell, A. H. Greenaway: Electron. Lett. **36,** 1358 (2000)
26. J. C. Baggett, T. M. Monro, W. Belardi, K. Furusawa, D. J. Richardson: Electron. Lett. **36,** 2065 (2000)

27. A. L. Gaeta: Conference on Lasers and Electro Optics (2001) Baltimore, Maryland, May 6-11, 2001, paper CMK3
28. J. H. V. Price, W. Belardi, T. M. Monro, A. Malinowski, A. Piper, D. J. Richardson: Opt. Express **10,** 382 (2002)

Figure captions

Fig. 1. Experimental configuration for characterizing supercontinuum extending into the UV.

Fig. 2. (a),(d) Numerically predicted intensity profiles (1dB contour spacing) and corresponding near-field photographs (produced by imaging the fiber end using a 100x microscope objective) for two-lobed spatial modes. (b) Calculated dispersion for fundamental and two-lobed spatial modes. (c) Calculated A_{eff} for the fundamental spatial mode. (Similar for two-lobed modes.) The solid and dashed curves are for the two principal polarization axes of the highly birefringent fiber.

Fig. 3. (a) Broadband supercontinuum spectrum extending from 300nm (UV) to 1600nm (IR). (b) Calculated efficiency of the UV optimized spectrometer. The spectrometer mirror efficiency (not shown) is 92% across the spectral range considered, and is included in the overall efficiency. (c) Transmission characteristics of the coloured filter used to eliminate unwanted long-wavelength scatter. (d) UV spectra from 300nm to 500nm recorded with and without coloured filter.

Fig. 4. (a) Experimental setup for de-tuning the launch into the holey fiber. (b) Far-field photographs of the colours produced in higher-order spatial modes. (i)-(iii) λpump = 820 nm; (iv)-(vi) λpump = 675 nm. The orientations of the modes correspond to those of the near field images in Fig. 2.

Fig. 5. Continuum spectra from coupling into two-lobed spatial mode (upper plots), and coupling into the fundamental mode (lower plots). Inset: photographs of corresponding far-field modes. (a) Wide span measurements. (b) Series of UV peaks at ~360nm. The coloured lines correspond to increasing pump pulse energy: +0, 1, 2, 3, 5, 6 dB with respect to the lowest intensity trace. (Due to different signal averaging times, quantitative comparison of upper and lower plots not possible.)

Fig. 6. Experimental (black) and theoretically modeled (red) supercontinuum spectra. (a) fundamental mode; (b) two-lobed mode (Fig. 2(d)).

Fig. 7. (a) Example far-field image observed when continuum produced in a subsidiary core of this multi-core fiber. (b)-(d) Near-field pictures showing continuum in principal and subsidiary cores, with overlaid SEM of fiber structure. Note that (b) and (c) are single pictures, whereas (d) is a composite image to show the variety of colours seen in different cores. The diamond shapes in (b) indicate the subsidiary cores in which we observed continuum generation.

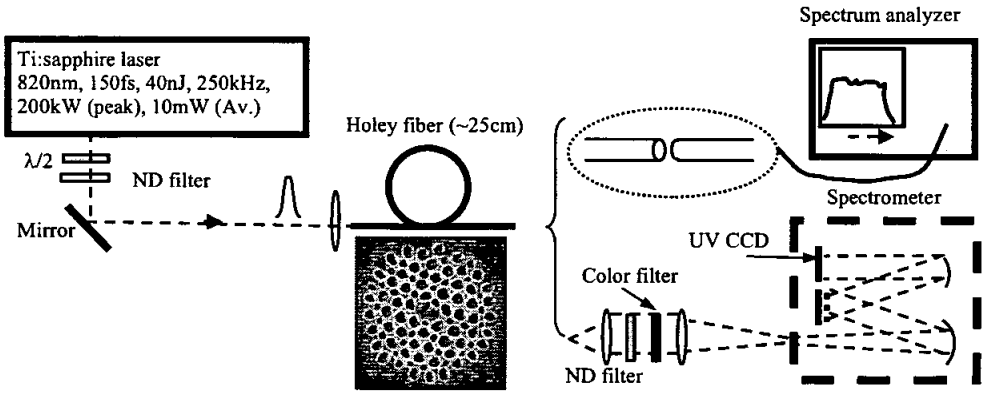
Spectrum analyzer
Ti:sapphire laser
820nm, 150fs, 40nJ, 250kHz,
200kW (peak), 10mW (Av.)
Holey fiber (~25cm)
λ/2
ND filter
Mirror
Spectrometer
UV CCD
Color filter
ND filter

Fig. 1.

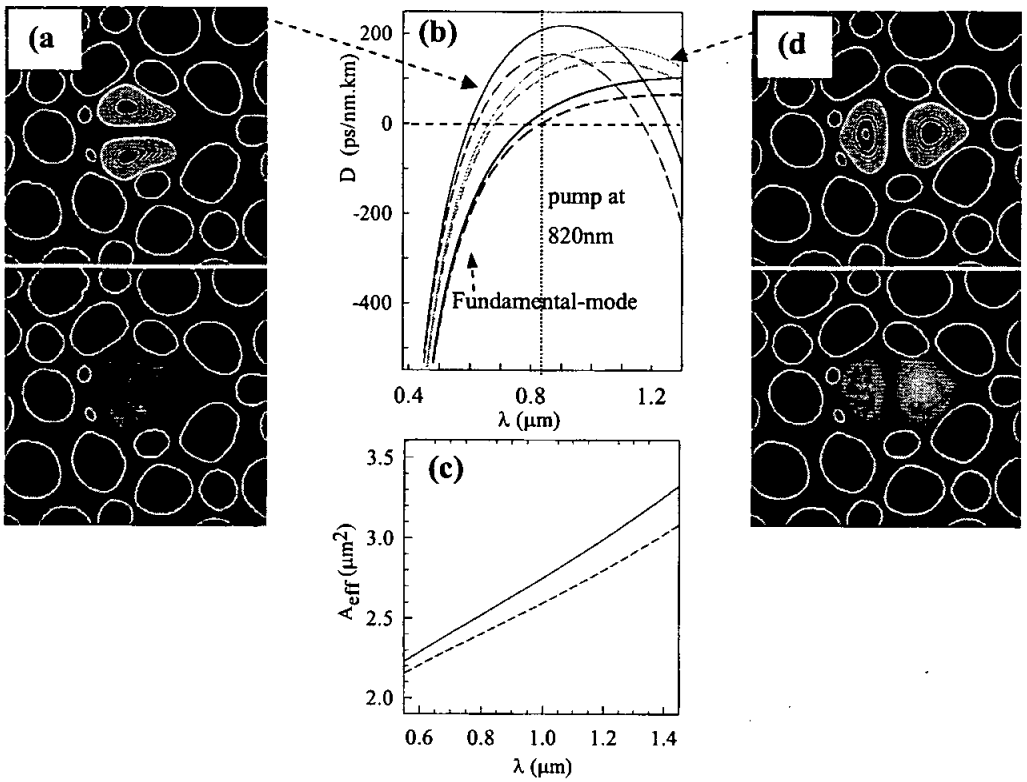
(a
(b)
(c)
(d
200
0
-200
-400
D (ps/nm.km)
pump at
820nm
Fundamental-mode
0.4
0.8
1.2
λ (μm)
3.5
3.0
2.5
2.0
A_{eff} (μm^2)
0.6
0.8
1.0
1.2
1.4
λ (μm)

Fig. 2.

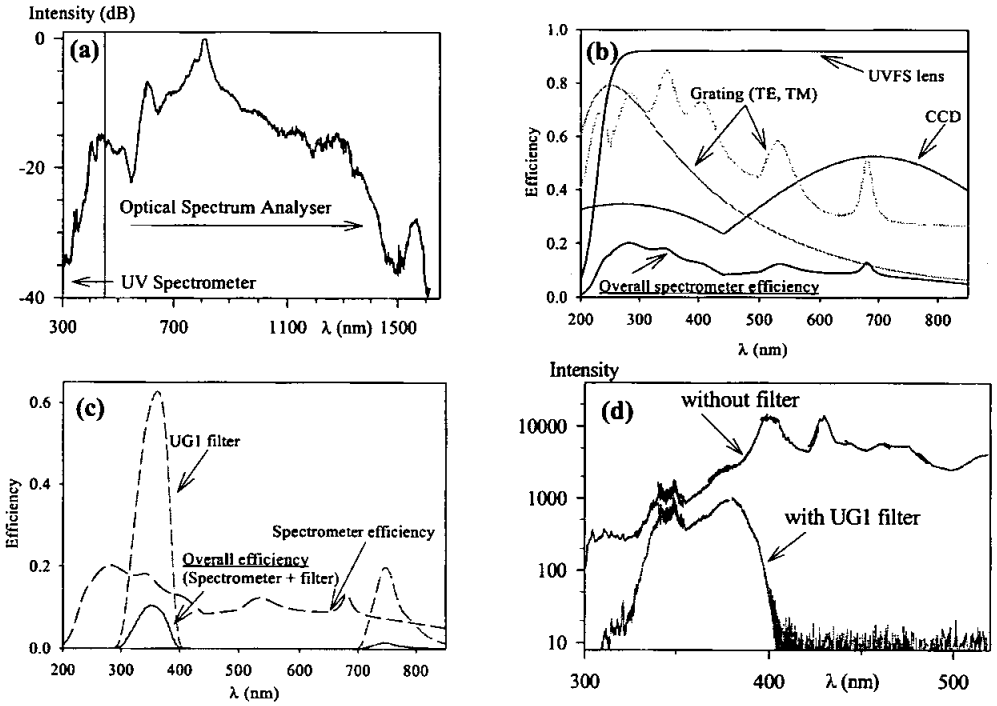
Intensity (dB)
(a)
Optical Spectrum Analyser
UV Spectrometer
λ (nm)
(b)
UVFS lens
Grating (TE, TM)
CCD
Overall spectrometer efficiency
Efficiency
λ (nm)
(c)
UG1 filter
Spectrometer efficiency
Overall efficiency
(Spectrometer + filter)
Efficiency
λ (nm)
Intensity
(d)
without filter
with UG1 filter
λ (nm)

Fig. 3.

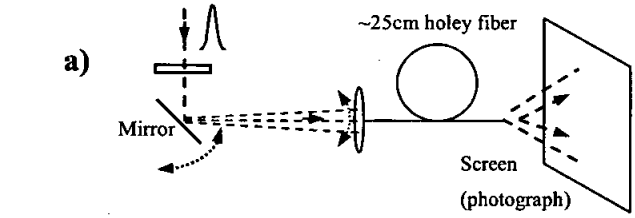

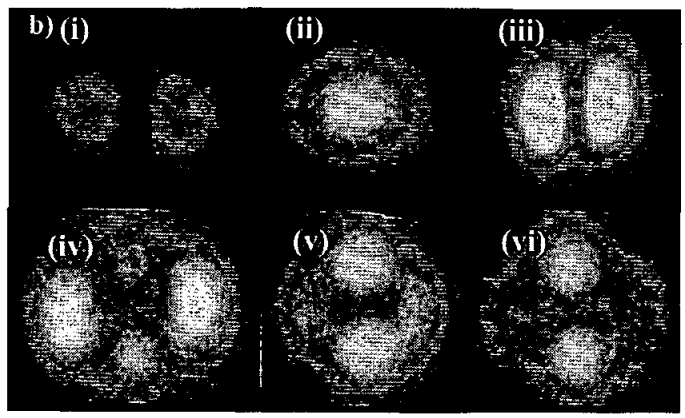

Fig. 4.

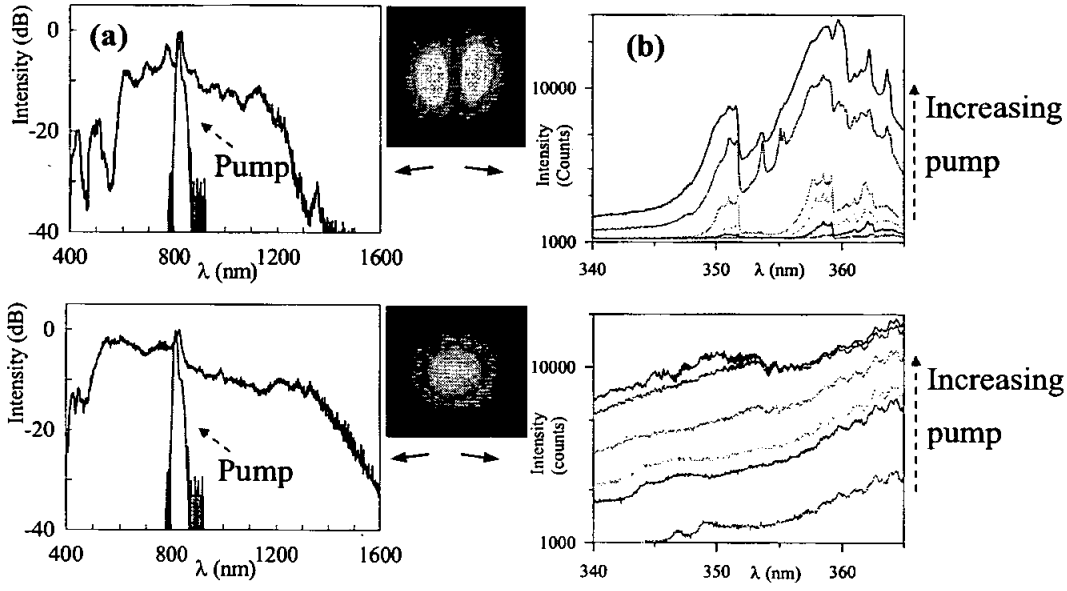
(a)
Intensity (dB)
0
-20
-40
Pump
400
800
1200
1600
λ (nm)
(b)
Intensity (Counts)
10000
1000
340
350
λ (nm)
360
Increasing pump
Intensity (dB)
0
-20
-40
Pump
400
800
1200
1600
λ (nm)
Intensity (counts)
10000
1000
340
350
λ (nm)
360
Increasing pump

Fig. 5.

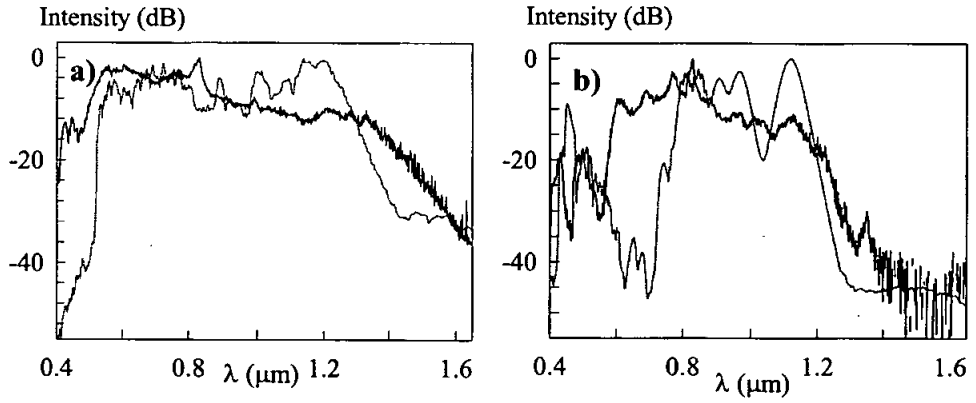
Intensity (dB)
0
-20
-40
a)
0.4
0.8
λ (μm)
1.2
1.6
Intensity (dB)
0
-20
-40
b)
0.4
0.8
λ (μm)
1.2
1.6

Fig. 6.

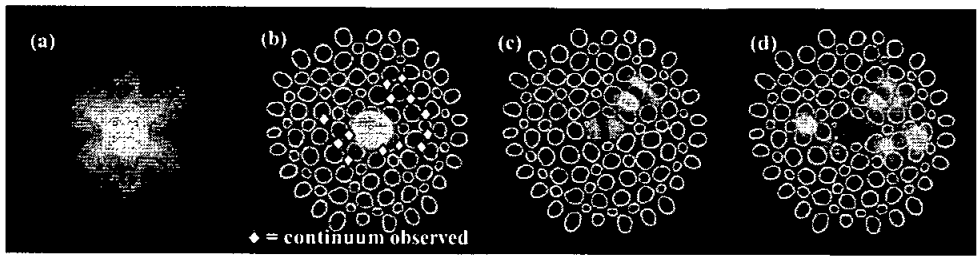

Fig. 7.